IET Microwaves, Antennas & Propagation

Research Article

IET Journals
The Institution of Engineering and Technology

Radar cross-section measurement in millimetre-wave for passive millimetre-wave identification tags

ISSN 1751-8725
Received on 21st April 2015
Revised on 8th July 2015
Accepted on 20th July 2015
doi: 10.1049/iet-map.2015.0281
www.ietdl.org

David Hotte[1] ✉, *Romain Siragusa*[1], *Yvan Duroc*[2], *Smail Tedjini*[1]

[1]*Laboratoire de Conception et d'Intégration des Systèmes, University Grenoble Alpes LCIS F-26900 Valence, 50 rue Barthélémy de Laffemas, 26902 Valence, France*
[2]*University Claude Bernard Lyon 1, Polytech Lyon, 15 boulevard André Latarjet, 69100 Villeurbanne, France*
✉ *E-mail: david.hotte@lcis.grenoble-inp.fr*

Abstract: The passive millimetre-wave identification (MMID) technology was introduced few years ago, exploiting the advantages of the passive ultra-high frequency (UHF) radio frequency identification (RFID). The communication is based on backscattering modulation, related to the radar cross-section (RCS) of the transponder. Thus, the need of accurate RCS measurement in the V-band arises. This work presents two methods to measure the RCS of any antenna in the particular case of MMID from 57 to 66 GHz. The studied methods require some precautions in millimetre-wave compared with measurements done in the UHF band. The two approaches highlight the methodology for accurate RCS measurement while the methods are evaluated through an example. A horn antenna is used as a MMID tag antenna and the RCS of the antenna is studied across three different loads as in UHF RFID: the short circuit, the open circuit and the matched load. The proposed methods provide a good accuracy and are validated by comparing the measurement results to the simulation.

1 Introduction

For many years, the radio frequency identification (RFID) technology has been intensively studied in different frequency bands and widely deployed across various applications such as logistics, localisation and supply-chain management [1]. RFID technology exhibits a lot of advantages such as low cost labelling without battery, long read range and embedded data memory. An RFID system is generally composed by a base station (reader) and a transponder (tag). The tag is composed by an antenna and an integrated circuit (IC), which is attached to the object to identify. In passive (or semi-passive) ultra-high frequency (UHF) RFID wireless communications, the tag responds to the base station by using the backscattering modulation. Therefore, the radar crosssection (RCS) is a key parameter to evaluate the performance of the RFID tag.

Few years ago, the millimetre-wave identification (MMID) concept has been introduced [2]. The main idea of MMID is to exploit the advantages of the UHF RFID technology in one part of the V-band from 57 to 66 GHz providing both a very large universal unlicensed frequency band and a solution for high-speed data rate as well as miniaturisation. The MMID principle was first proven with a passive UHF RFID communication transposed at 10 GHz having a read range of 30 cm [3]. At 60 GHz, a MMID reader has been fabricated on 90 nm CMOS and LTCC technology [4] while some tags based on patch antenna array have been designed and tested [5, 6]. An antenna gain from 11.1 to 18 dBi is reached while the −10 dB impedance bandwidth varies from 1 to 3.8 GHz. For each tag, the antenna area is smaller than few square centimetres.

The MMID concept is the same as UHF RFID, but some specific properties appear around 60 GHz compared with the UHF band. The MMID tag is smaller than the UHF tag and thus the reading is much more sensitive to the position of the tag as well as its orientation. In addition, the signal levels are more attenuated because the propagation losses are higher while the power of millimetre sources are limited to about 25 dBm. As a consequence, even if the antennas in V-band are directive, the read range of MMID will be significantly shorter. Therefore, the RCS parameter becomes even more sensitive than in UHF and more difficult to measure.

The RCS measurement of any object or any antenna can be made with a radar system or with a vector network analyser (VNA), which is the most frequently used technique. The RCS measurement applied for UHF RFID tags is similar to radar measurement, but the RCS does not depend only on the tag antenna geometry but also on the impedance of the RFID chip. Two usual techniques using VNA exist to characterise RFID tags RCS in function of the load. One technique consists on computing the RCS by applying the radar equation [7–9] to the backscattered power while removing the contribution of the antenna mount and the environment backscattering. These parasitic effects can be removed with different methods, such as modelling these contributions or subtracting the response without the target to the response with the target [10]. The other usually used RCS measurement technique is to measure the backscattered power from a reference target for which RCS is known and to compare it with the received power from the antenna under test [10]. However in the case of MMID tags, the translation of these methods is not direct and requires specific and additional attentions to accurately measure RCS. In particular, the time gating technique [11] has to be used to accurately separate the different echoes that are close to each other because of small distances of measurement in the millimetre-wave band.

The objective of this paper is to present two RCS measurement techniques in the V-band while the proposed methodology is validated from an example. After recalling the principle of backscattered communications in passive RFID and MMID systems, Section 2 highlights the difficulties for the RCS measurement in MMID with some examples. Section 3 details the two procedures for the RCS measurement using the radar equation and then a reference target, highlighting all specific recommendations for MMID tags. Section 4 focuses on the S-parameters measurement and their exploitation to deduce the RCS and describes how to use effectively the time gating technique. The analysis is illustrated using a loaded linearly polarised horn antenna. Section 5 compares the results achieved for the RCS determination of the horn antenna: RCS calculated in simulation and RCS deduced from measurement with the two proposed methods. Finally in Section 6, some conclusions are drawn.

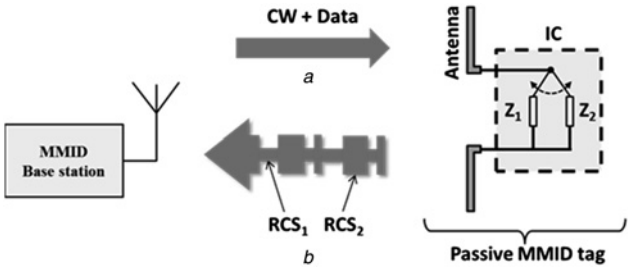

Fig. 1 *Illustration of passive MMID communication*

a Downlink step where the reader sends a CW and data
b Uplink step with RCS_1 and RCS_2 corresponding respectively to each load Z_1 and Z_2

2 Radar cross-section in millimetre-wave identification

Based on the same principle as in passive RFID, the passive MMID communication between the reader and the tag is realised in two steps as illustrated on Fig. 1. First, the reader sends power and data to the tag during the downlink step. Then, during the uplink step the tag responds to the reader by using the backscattering modulation.

During the downlink step, the reader feeds the passive tag because it does not embed any source of energy. During the uplink step, the IC switches between the two loads Z_1 and Z_2 while the reader sends a continuous wave (CW). Each load corresponds to one RCS and an associated level of backscattered signal as presented in Fig. 1*b*.

Compared with UHF RFID signals, the power level of MMID signals is much lower. Indeed, on one hand, the propagation losses are higher, and on the other hand, the RCS is lower than in the UHF band. For example, at one metre the propagation losses in free space are −31 dB at 868 MHz and −68 dB at 60 GHz.

Moreover, the maximum RCS of a dipole tag, that is, when the dipole is loaded by a short circuit, is about −15 dBm² in UHF and lower than −50 dBm² in MMID. To compensate the high propagation losses, the millimetre-wave tag antennas are much more directive [6] (antennas arrays from 10 to 18 dBi) than the UHF ones (single dipole with a gain of about 2 dBi). The high directivity requires a perfect alignment between the reader and tag antennas.

Thus the weak level of MMID signals and the needed alignment of antennas lead to pay special attention to the RCS value and its measurement.

3 Radar cross-section measurement

3.1 Measurement bench using vector network analyser

The common RCS measurement technique consists in the far-field measurement of the power sent back by the target, which is the tag for the considered application, using the S-parameters acquired with a VNA. As illustrated in Fig. 2 (where *Tx* refers to the transmission and *Rx* refers to the reception), two configurations are possible: the bi-static setup with two antennas [12], one antenna for transmission and one antenna for reception; the mono-static setup with only one antenna for transmission and reception [7]. The power transfer is characterised by the transmission coefficient in bi-static setup and the reflection coefficient in mono-static setup.

The remainder of this section outlines the advantages and drawbacks of each configuration to measure the RCS of MMID tags.

3.1.1 Bi-static configuration: In the bi-static configuration (Fig. 2*a*), the emitted wave has an incident angle φ. For RFID tags, this angle does not affect the measured RCS because the radiation pattern of the tag is quasi-omnidirectional [9]. However in MMID, this angle strongly influences the measurement because the tag antennas are directive. Even considering a small angle φ, the error could reach several decibels while the setup is unrealisable in practice; the distances increasing and the theoretical MMID maximum communication distance being about one metre [2]. Thus, the bi-static configuration for directive MMID tag antennas is not suitable for measurement. If the target responds in cross-polarisation, a dual-linearly polarised antenna can be used as probe, while avoiding the environmental contribution such as in [13] and overcoming the incident angle issue. In this configuration, the isolation between the two ports of the antenna will be a critical parameter for the accuracy. However in the studied case the target is a linearly polarised antenna which responds in co-polarisation (as well as most of UHF tags), hence the use of a dual-polarised antenna is not suitable.

3.1.2 Mono-static configuration: The mono-static setup (Fig. 2*b*) solves the issues relied to the antennas alignment and the minimum incident angle. However the setup introduces the superposition of the reflected wave from the *Tx*/*Rx* antenna to the backscattered wave from the target and the measurement is very sensitive to the spurious reflections from the environment [10]. A time gating [11] allows the separation in time domain of the reflected and backscattered waves, and any other time separated parasitic responses. This processing makes possible the separation

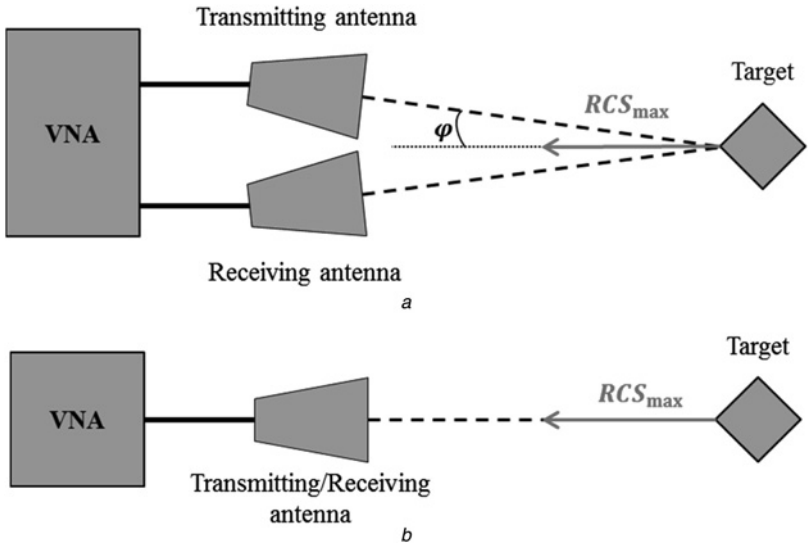

Fig. 2 *Configurations of the two possible measurement benches*

a Bi-static (measurement of the S_{21} parameter)
b Mono-static (measurement of the S_{11} parameter)

of the target response and ensures a good accuracy in the RCS measurement at millimetre-waves. The mono-static configuration, combined to time gating, is chosen for the MMID tag characterisation.

3.1.3 Measurement bench in mono-static setup: The mono-static setup is shown in Fig. 3. The *Tx/Rx* antenna is a WR15 horn antenna of aperture 21 mm × 18 mm, with a gain from 19 to 22 dBi in the V-band. The S-parameters are acquired by the Agilent N5222A VNA and a Virginia Diodes WR15-VNAX 50–75 GHz VNA extension (VDI module). The VDI module is a frequency multiplier combined to a mixer with a rectangular waveguide WR15 output. The same horn antenna as for the *Tx/Rx* one is chosen as AUT for its complex 3D structure and high directivity to validate all of the presented measurement methods.

A short-open-load calibration process is performed at the output of the VDI module and a sensitivity of −65 dBm is reached. The distance between the *Tx/Rx* antenna and the horn antenna target is fixed to 50 cm, distance complying with far-field conditions, time domain separation of the responses and VNA sensitivity. It should be noted that the measurements can be performed without an anechoic chamber thanks to the low level of parasitic signals and the absence of other 60 GHz sources. More complex assembly (with lens for focusing the signal or a near-field configuration) is unnecessary because the MMID tag antennas size is compliant with the far-field condition and positioning accuracy while the directive antennas ensure a sufficiently high power to be detected.

3.2 Method for radar cross-section measurement

The two methods to measure the RCS, the first one based on the radar equation [7] and the second one using a calibration process [10], are detailed in this section with the same objective: to take into account the millimetre-wave context and to highlight the differences with the measurements for UHF RFID tags. In this part, it should be noted that the reflection coefficients are supposed accurately measured; Section 4 will detail the procedure to follow.

3.2.1 RCS measurement using radar equation: The RCS can be determined by measuring the backscattered power and using the radar equation. This method is widely used in UHF RFID tag characterisation and provides an accuracy of few decibels at the tag's resonance [7]. Using the radar equation for mono-static case, the backscattered power P_b is given by (1)

$$P_b = P_e G_h{}^2 \frac{\lambda^2}{(4\pi)^3 R^4} \sigma_{target} \left(1 - \left|S_{11}^{Tx/Rx}\right|^2\right)^2, \quad (1)$$

where P_e is the output power of the VDI module, $S_{11}^{Tx/Rx}$ is the *Tx/Rx* antenna reflection coefficient, G_h is the *Tx/Rx* horn antenna gain, λ is the wavelength, R is the distance between the *Tx/Rx* antenna and the target and σ_{target} is the RCS of the target, which is the antenna to characterise.

Usually and notably in UHF RFID, the reflection coefficient of the *Tx/Rx* antenna is not taken into account in the radar formula because the power transfer $PT = \left(1 - \left|S_{11}^{Tx/Rx}\right|^2\right)$ is very close to unity. However in MMID, the approximation is not suitable because the backscattered signals are very low regarding the reflection coefficient of the *Tx/Rx* horn antenna. For example, with a distance $R = 50$ cm and a *Tx/Rx* antenna with a gain of 20 dBi at 60 GHz, the power ratio is about −42 dB which is very low compared with the $S_{11}^{Tx/Rx}$ that is around −30 dB in the entire band. Ignoring the power transfer in (1), the error on P_b could be up to 0.1 dB with a $S_{11}^{Tx/Rx}$ equals to −20 dB.

Three measured reflection coefficients are required to calculate the target RCS:

- $S_{11}^{Tx/Rx}$, which is necessary to quantify the exact transmitted/received power to the VNA.

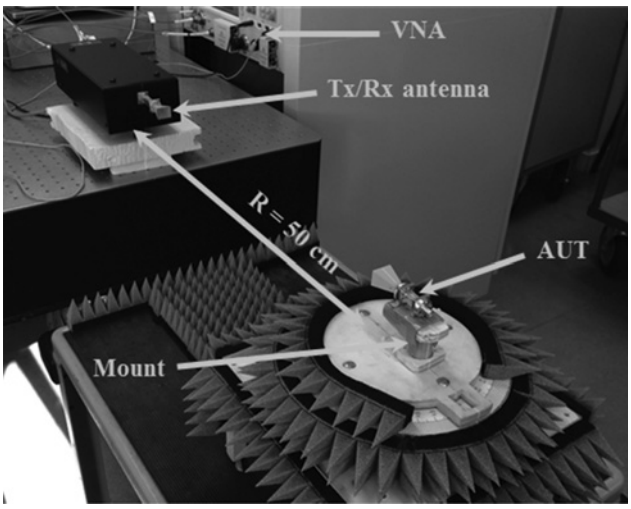

Fig. 3 *Mono-static setup for the measurement of a loaded horn antenna RCS from 57 to 66 GHz. The Tx/Rx antenna and the AUT put on the mount are aligned with a laser beam*

- S_{11}^{m}, when the target mount is in place. This measurement includes the reflection from the mount and the reflection of the *Tx/Rx* antenna, quantifying the environment noise and internal reflections.
- S_{11}^{target}, which is obtained when the target is attached to its mount in front of the *Tx/Rx* antenna.

The power ratio P_b/P_e is computed with (2) by eliminating the mount contribution.

$$\frac{P_b}{P_e} = \left|S_{11}^{target} - S_{11}^{m}\right|^2 \quad (2)$$

The RCS of the targeted AUT is then calculated with (3) by combining (1) and (2).

$$\sigma_{target} = \left|S_{11}^{target} - S_{11}^{m}\right|^2 \frac{(4\pi)^3 R^4}{G_h^2 \lambda^2 \left(1 - \left|S_{11}^{Tx/Rx}\right|^2\right)^2} \quad (3)$$

This method presents the advantage of simplicity and the measurement does not require any reference target for calibration process. However it supposes that all of the parameters of the radar equation are known with a good accuracy and notably the *PT*.

3.2.2 RCS measurement using reference target: The second method is to use a reference target with a known RCS which allows performing a calibration process taking into account every parameter of the transmission, including the mount contribution as well as other clutters or parasitic effects. The procedure requires three measured reflection coefficients to calculate the target RCS:

- S_{11}^{m}, when the mount is placed in front of the *Tx/Rx* antenna, such as for the previous method.
- S_{11}^{ref}, which is the power ratio when the reference target is placed on its mount.
- S_{11}^{target}, when the target is placed on the mount.

The setup of the measurement is the same as the previous method: a mono-static configuration with the *Tx/Rx* horn antenna separated from the target by a distance of 50 cm. The power ratios are corrected by subtracting S_{11}^{m} using (2) to remove parasitic contributions. The RCS of the target is obtained using (4), with

σ_{ref} the reference target RCS.

$$\sigma_{target} = \frac{\left|S_{11}^{target} - S_{11}^{m}\right|^2}{\left|S_{11}^{ref} - S_{11}^{m}\right|^2}\sigma_{ref} \quad (4)$$

Contrarily to the previous method, this technique does not require to know the full acquisition chain. However, the reference target is a critical parameter: an error on the reference measurement will strongly affect the RCS of the target under test. In addition, a trade-off has to be done in the choice of the reference target. In UHF band, the common references are either sphere of radius r with a RCS, σ_{sphere}, either a flat plate of surface S with a RCS, σ_0. The corresponding theoretical RCS are given by (5) and (6)

$$\sigma_{sphere} = \pi r^2 \quad (5)$$

and

$$\sigma_0 = 4\pi\frac{S^2}{\lambda^2} \quad (6)$$

In the UHF band, the sphere is the most used because its RCS has a strong enough level, independent of the frequency and it exhibits an isotropic pattern. Nevertheless in the V-band, these sizes of sphere are not convenient as the far-field criterion will be around few metres, which is not suitable for the measurement setup. A good trade-off between the far-field criterion and the RCS level is the flat plate, which can be easily fabricated contrary to the sphere. However, the plate RCS σ_{plate} depends on the incident angle θ [14], as seen in (7)

$$\sigma_{plate} = \sigma_0\left(\frac{\sin\left(2\pi/\lambda a\sin\theta\right)}{2\pi/\lambda a\sin\theta}\right)^2\cos\theta^2, \quad (7)$$

where σ_0 is the RCS calculated using (6) at normal incidence and a is the dimension of the plate in the polarisation of the incoming linearly polarised wave. An important error can be integrated in the RCS calculation if the plate is not perfectly aligned with the *Tx*/*Rx* horn antenna. For example, the simulated RCS at 60 GHz of a square plate of 3 cm × 3 cm is decreased by 1 dB while the plate is rotated by only 1.2°. In conclusion, the sphere is better for its isotropic RCS pattern but the low level of RCS is more constraining than the angle dependency of the flat plate, which provides a very high level of RCS.

In the following, a flat square plate of 3 cm × 3 cm is chosen. This is a good trade-off between far-field condition at 50 cm and the RCS level approximately equals to −4 dBm² at 60 GHz. In comparison, a sphere of diameter 3 cm has a RCS only of −31.5 dBm². It should be noted that the impact on the RCS of the flatness and smoothness of the plate is supposed negligible. Indeed, the manufacturing process of printed card board presents an accuracy of 2.5 µm for a 35 µm copper thickness, compared with the 60 GHz wavelength which is 5 mm.

4 Reflection coefficients measurement

The calculation of the RCS requires the accurate knowledge of the reflection coefficients as presented in previous section. This section focuses on the reflection coefficients measurement notably highlighting the influence of time gating on the accuracy. The final objective is to determine the RCS of the AUT loaded by three standards loads (short circuit [SC], open waveguide [OW] and matched load [ML]). The simulation models, the fundamentals of time gating and the reflection coefficients measurement results are presented. The simulations are performed with CST Microwave Studio 2012 based on the finite integration technique.

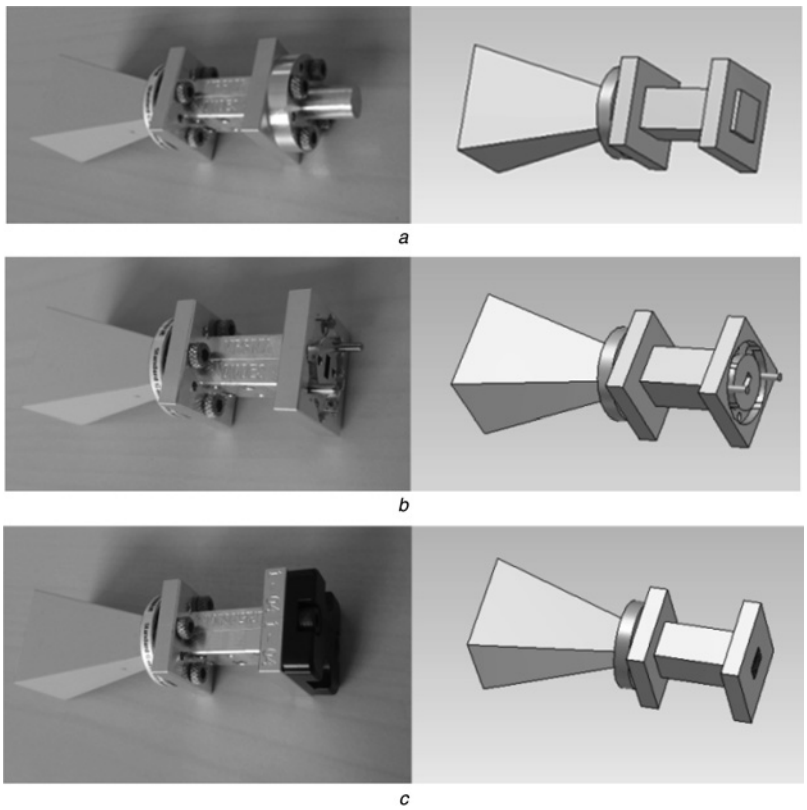

Fig. 4 *AUT: a horn antenna of rectangular aperture 21 mm × 18 mm and the three different measured configurations (left-hand side) and the associated simulation model (right)*

a Short circuit
b Open waveguide
c Matched load

IET Microw. Antennas Propag., 2015, Vol. 9, Iss. 15, pp. 1733–1739

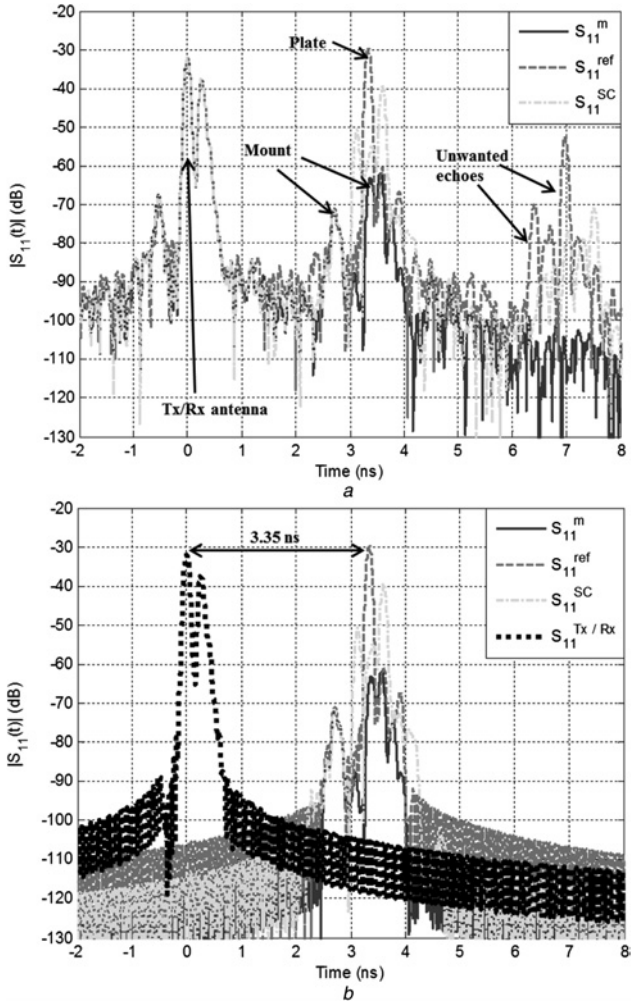

Fig. 5 *Measured reflection coefficient in time domain of the Tx/Rx antenna in front of: the support, the reference plate and the SC case*

a Before time gating
b After time gating

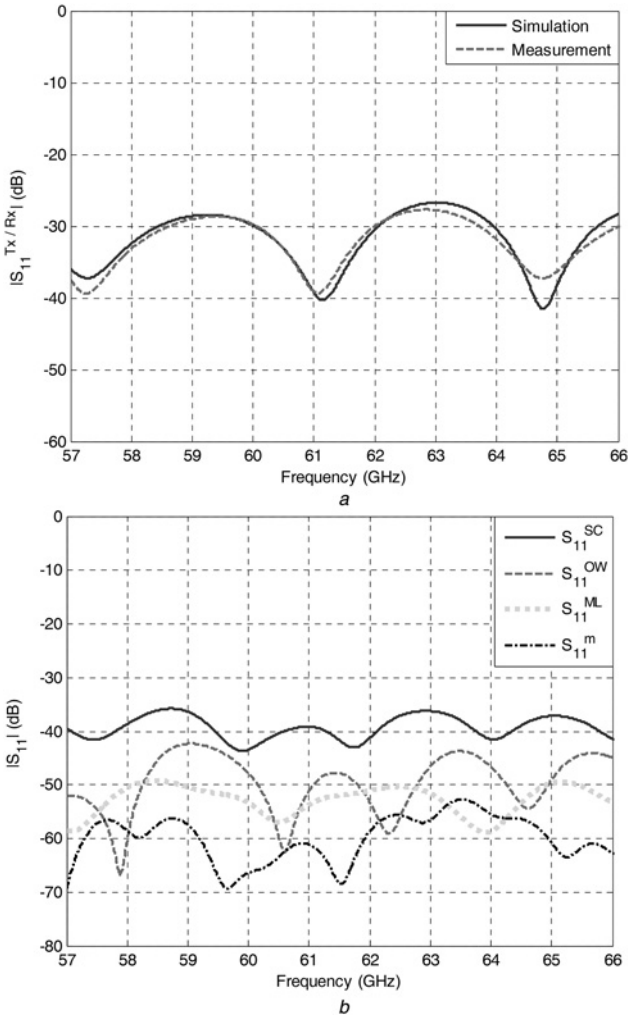

Fig. 6 *Measured reflection coefficients used in the RCS calculation*

a Simulated and measured reflection coefficient $S_{11}^{Tx/Rx}$ of the horn antenna
b S_{11} for the three configurations (horn antenna loaded by SC, OW, ML) and the mount without any target (m)

4.1 Measured configurations and their simulation models

Fig. 4 shows the photographs of the AUT connected to the three loads and the associated CST Microwave Studio models. The loads are connected to the AUT with a straight rectangular waveguide WR15 with standard section of 3.76 mm × 1.88 mm and a length of 25.4 mm. The SC (Fig. 4*a*) is realised by ending the waveguide with a plate. As the open circuit, load usually used the theory of RCS in UHF RFID, being not realisable in rectangular waveguide, it is replaced by the open waveguide (Fig. 4*b*). In theory, it is not a real open condition (i.e. reflection coefficient equal to 1) because the waveguide impedance is near to the vacuum impedance: the guided wave will be radiated at the waveguide opening. This is confirmed by simulation where a return loss of −13 dB at 60 GHz is obtained when the source port is one waveguide terminal and the other terminal is not connected. The ML (Fig. 4*c*) is realised by using the broadband load of the VDI module calibration kit.

It should be noted that the flange of connection of the waveguide (a square of side 19 mm) is integrated in the simulation because its dimensions have a strong effect on the RCS, especially the alignment pins in the OW case which impact the resonant frequency (with a frequency shift up to 200 MHz). For each configuration, the RCS in the main beam direction is simulated and will be presented with measurement results for comparison (Fig. 8).

4.2 Considerations on the time gating

The time gating has to be carefully processed because it can introduce errors as offset, distortion and edge effect [15]. Three main parameters have to be considered: the temporal span allows the adjustment of the window width to the desired response while a trade-off exists between the cut-off time and the side lobe level (SLL) of the window [16] (the higher is the cut-off time, the lower is the SLL). The choice of the cut-off time and the SLL will depend on the characteristics of the response and its environment, that is, the other echoes. Obviously, as the target response is *a priori* not known, the different adjustments result on the knowledge and expertise of the operator. The temporal span notably has to lock onto the widest time response between the support and the target to limit the edge effect. If there is overlapping on the desired response, it is possible to modify the distance between the target and reflection sources, or with more efficiency to integrate the bench in a controlled environment.

In the presented results, the time gating function available in the VNA is used: the measurement uncertainty due to the flatness is ±0.1 dB and the SLL is from −48 to −70 dB. Fig. 5 shows different S_{11} measurements in time domain before (Fig. 5*a*) and after (Fig. 5*b*) time gating.

The separating distance between the *Rx*/*Tx* antenna and the target is 50 cm, ensuring far-field conditions and no overlapping while the backscattered power for the minimal RCS is higher than the VNA sensitivity. As the AUT is not resonant and the levels of unwanted

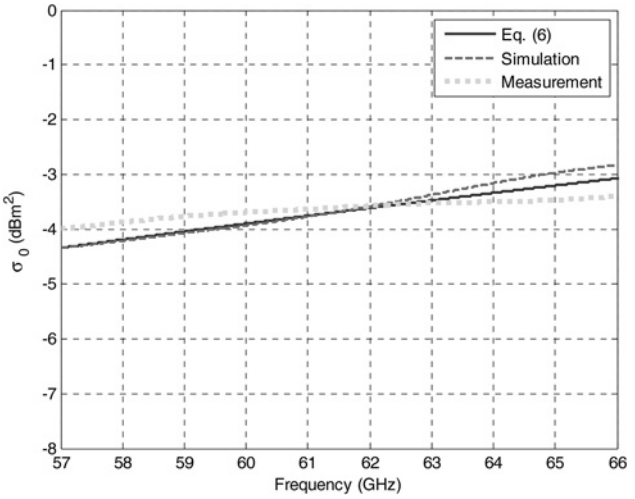

Fig. 7 *Reference target RCS using full wave simulation, calculation from the theoretical formula (6), and calculation from the measured reflection coefficient and (3)*

echoes are high compared with the target, the rejection level is maximised (−70 dB of SLL) to the detriment of the cut-off time (706 ps). The temporal span is set to 2.031 ns corresponding to the support response, which is wider than the target response.

The *Tx*/*Rx* antenna response is isolated from the ungated S_{11}^{m} curve by applying a window centred on the *Tx*/*Rx* echo. The round-trip time between the *Tx*/*Rx* antenna and the target is 3.35 ns corresponding to 50 cm of spacing. All the parasitic echoes are clearly visible in Fig. 5*a*. For example, the reflection of the *Tx*/*Rx* antenna and the unwanted echoes are parasitic responses for the plate RCS measurement. After time gating, all of these echoes vanished and only the response of the plate on the support is measured (Fig. 5*b*, dash line).

4.3 Application to the reflection coefficients measurement

The reflection coefficients are accurately measured by taking into account the described dispositions and compared with simulation results. The measured reflection coefficients used in the RCS calculation are presented in Fig. 6. The measured and simulated $S_{11}^{Tx/Rx}$ are compared in Fig. 6*a*. The results show a very good agreement and validate the measurement procedure using time gating technique. The reflection coefficients for the three different loads and the support are compared together in Fig. 6*b*.

As expected, the reflection coefficient is the strongest when a short circuit is connected to the AUT. The mount backscattering level is closed to the ML or OW cases and thus the mount has a strong impact on the calculation of the RCS for the ML and OW load. However the mount contribution is negligible for the SC case that is at least 20 dB upper.

5 Radar cross-section measurement of a loaded horn antenna

Based on the two methods of RCS calculation (Section 3) and the accurate measurement of reflection coefficients, this section presents the RCS of the horn antenna loaded by the three loads. The main objective is to validate the full procedure comparing simulation and measurement.

Beforehand, the RCS of the flat plate used as reference target is determined to use the method described in Section 3.2. Three approaches are compared: calculation from the theoretical formula (6), full simulation, and calculation from the measured reflection coefficient and (3). Fig. 7 presents the different results that are in

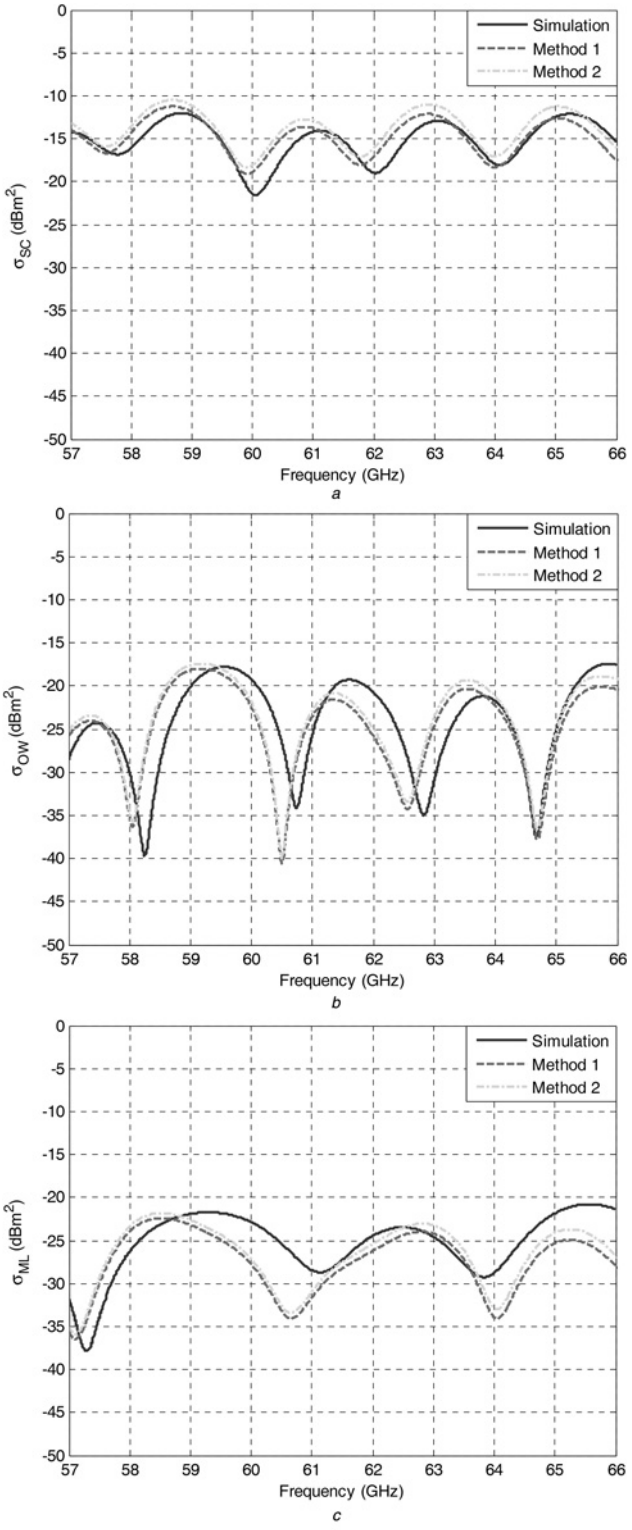

Fig. 8 *RCS of the loaded horn antenna. Comparison between full wave simulation and the two methods. Method 1 refers to (3) and method 2 refers to (4)*

a Short circuit
b Open waveguide
c Matched load

good agreement with a maximum error of 0.35 dB and a relative error between −7 and 8%.

Finally, Fig. 8 presents the simulated and measured RCS for the three loads: σ_{SC} is the short circuit case (Fig. 8*a*), σ_{OW} is the open waveguide case (Fig. 8*b*) and σ_{ML} is the matched load case

IET Microw. Antennas Propag., 2015, Vol. 9, Iss. 15, pp. 1733–1739

Table 1 Estimated accuracy of each method

Accuracy	Method 1		Method 2
positioning error		±0.9 dBm²	
time gating error		±0.1 dB	
Tx/*Rx* gain	±0.1 dB		–
path loss	±0.1 dB		–
positioning error on reference target	–		±0.35 dBm²
total	±1.2 dB		±1.35 dB

(Fig. 8*c*). The simulated RCS are obtained with a RCS far-field monitor. 'Method 1' refers to the RCS calculation using (3) and 'Method 2' refers to the calculation using (4).

Measurement and simulation are in good agreement. The two proposed methods for RCS measurement present a maximum difference of only 1 dB in all considered cases and validate each other. The most critical factor of error is the positioning. As noted during the measurement process, a small deviation can affect the level of signal as well as the resonance frequencies. The time gating technique can also introduce some errors but they are negligible in comparison with the positioning error. In Fig. 8*c*, differences in the amplitude between two consecutive extremes from 64 to 66 GHz are observed. These differences are due to misalignment and to the electromagnetic model of the matched load in the simulation software. In the simulation, the matched load is modelled as a waveguide port, which is perfectly matched to the waveguide in the entire frequency band. However, the real waveguide load is composed by a shorted waveguide with a specific absorber at the end. Therefore, the matching is not the same as in the simulation.

The measurement uncertainty can be estimated for both methods and mainly comes from the positioning and the time gating. The angular positioning on the bench is about ±1°: in practice, a specific laser is used for the alignment. By evaluating the simulated 3D RCS pattern of each studied case, the positioning accuracy induces a maximum uncertainty of ±0.9 dBm². Supposing that the window span is correctly set to extract the significant signal, the time gating adds a measured maximum uncertainty of ±0.1 dB on the reflection coefficient due to the flatness of the window. In method 1, two other factors are included: the *Tx*/*Rx* gain accuracy (±0.1 dB from the datasheet), and the distance R (measured with ±1% of accuracy leading to ±0.1 dB in the path losses). In method 2, the uncertainty on the reference RCS is about ±0.35 dBm². The uncertainty in method 1 is about ±1.2 dB while the uncertainty is about ±1.35 dB in method 2. This accuracy analysis is summarised in Table 1. A maximum shift in frequency of ±440 MHz due to positioning is also observed in Fig. 8*c*, corresponding to 0.7% of 60 GHz, a common value in millimetre-wave antennas measurement. Therefore all results are valid regarding to the approximated accuracy of measurement.

6 Conclusion

This work presents two methods to measure the RCS of any antenna in millimetre band in the particular case of MMID. The RCS is a fundamental parameter in MMID whose measurement requires particular precautions compared with RFID case: as shown, an approximate alignment or a bi-static measurement could notably lead to an important error. For the two approaches, the measurement methodology is underlined. The presented results show that the critical RCS parameter in MMID can be accurately measured from 57 to 66 GHz. It should be noted that the presented measurement protocols are valid at any frequency band and do not require inevitably an anechoic chamber.

7 References

1 Finkenzeller, K.: 'Rfid handbook: fundamentals and applications in contactless smart cards and identification' (John Wiley & Sons Inc., USA, New York, 2003, 2nd edn.)
2 Pursula, P., Vähä-Heikkilä, T., Müller, A., *et al.*: 'Millimeter-wave identification-A new short-range radio system for low-power high data-rate applications', *IEEE Trans. Microw. Theory Techn.*, 2008, **56**, (10), pp. 2221–2228
3 Pursula, P., Donzelli, F., Seppä, H.: 'Passive rfid at millimeter waves', *IEEE Trans. Microw. Theory Techn.*, 2011, **59**, (8), pp. 2151–2157
4 Pursula, P., Karttaavi, T., Kantanen, M., *et al.*: '60-GHz millimeter-wave identification reader on 90-nm CMOS and LTCC', *IEEE Trans. Microw. Theory Techn.*, 2011, **59**, (4), pp. 1166–1173
5 Kiuru, T., Pursula, P., Rajamäki, J., *et al.*: 'A 60-GHz semipassive mmid transponder for backscattering communication'. IEEE MTT-S Int. Microwave Symp. Digest, Seattle, WA, June 2013, pp. 1–3
6 Pursula, P., Donzelli, F.: 'Transponders for millimeter wave identification'. IEEE-APS Topical Conf. Antennas Propagation Wireless Communicaton, Torino, Italy, September 2011, pp. 1221–1224
7 Nikitin, P.V., Rao, K.V.S.: 'Theory and measurement of backscattering from rfid tags', *IEEE Trans. Antennas Propag.*, 2006, **48**, (6), pp. 212–218
8 Hess, D.W.: 'Introduction to rcs measurements'. Antennas Propagation Conf. 2008, Loughborough, UK, March 2008, pp. 37–44
9 Pouzin, A., Vuong, T.-P., Tedjini, S., *et al.*: 'Measurement of radar cross-section for passive uhf rfid tags'. Second European Conf. Antennas Propagation, Edinburgh, UK, November 2007, pp. 1–6
10 Ali, A.S., Deats, B.W.: 'Modeling system reflections to quantify rcs measurement errors'. 15th Annual Meeting and Symp. Antenna Measurement Techniques Association, Dallas, Texas, October 1993, pp. 445–450
11 Shoulders, B., Betts, L.: 'Advancements in millimeter wave gated rcs measurements'. 28th Annual Meeting and Symp. Antenna Measurement Techniques Association, Austin, Texas, USA, October 2006, pp. 360–365
12 Miacci, M.A.S., Nohara, E.L., Martin, I.M., *et al.*: 'Indoor radar cross section measurements of simple targets', *J. Aerosp. Technol. Manage.*, 2012, **4**, (1), pp. 25–32
13 Vena, A., Perret, E., Tedjini, S., 'A depolarizing chipless rfid tag for robust detection and its fcc compliant uwb reading system', *IEEE Trans. Microw. Theory Techn.*, 2013, **61**, (8), pp. 2982–2994
14 Brooker, G.: 'Chapter 8 – target and clutter characteristics', in Brooker, G. (Ed.): 'Introduction to sensors for ranging and imaging' (SciTech Publishing Inc., Raleigh, USA, 2009, 1st edn.)
15 Henderson, A., James, J.R., Newham, P., *et al.*: 'Analysis of gating errors in time domain antenna measurements', *IEEE Trans. Antennas Propag.*, 1989, **136**, (4), pp. 311–320
16 Agilent: 'Time domain analysis using a network analyzer', Appl. Note 1287–12, pp. 1–48